PICTURE OF THE MONTH

⌀Rapid Scan Visible Imagery from the Geostationary Lightning Mapper (GLM) at 2.5-Minute Intervals✎

Daniel J. Cecil,[a] Dennis E. Buechler,[b] John R. Mecikalski,[c] and Xuanli Li[b]

[a] *NASA Marshall Space Flight Center, Earth Science Branch, Huntsville, Alabama*
[b] *Earth System Science Center, University of Alabama–Huntsville, Huntsville, Alabama*
[c] *Atmospheric and Earth Science Department, University of Alabama–Huntsville, Huntsville, Alabama*

ABSTRACT: The Geostationary Lightning Mapper (GLM) is an instrument designed to continuously monitor lightning. It is on the *GOES-16* and *GOES-17* satellites, viewing much of the Western Hemisphere equatorward of 55°. Besides recording lightning-flash information, it transmits background visible-band images of its field of view every 2.5 min. The background images are not calibrated or geolocated, and they only have ~10-km grid spacing, but their 2.5-min sampling can potentially fill temporal gaps between full-disk imagery from the GOES satellites' Advanced Baseline Imager. This paper applies an initial calibration and geolocation of the GLM background images and focuses on animations for two cases: a volcanic eruption in Guatemala and a severe thunderstorm complex in Argentina. Those locations typically have 10-min intervals between full-disk scans. Prior to April 2019, the interval was 15 min. Despite coarse horizontal resolution, the rapid updates from GLM background images appear to be useful in these cases. The 3 June 2018 eruption of Fuego Volcano appears in the GLM background imagery as an initial darkening of the pixels very near the volcano and then an outward expansion of the dark ash cloud. The GLM background imagery lacks horizontal textural detail but compensates for this lack with temporal detail. The ash cloud resembles a dark blob steadily expanding from frame to frame. Animation of the severe thunderstorm scene reveals vertical wind shear, with northerly low-level flow across a growing cumulus field and west-northwesterly upper-level flow at anvil level. Convective initiation is seen, as are propagating outflow boundaries and overshooting convective cloud tops.

KEYWORDS: Volcanoes; Thunderstorms; Satellite observations

1. Introduction

The GOES-R satellite series features two new instruments, the Advanced Baseline Imager (ABI) and Geostationary Lightning Mapper (GLM), having a wealth of uses for weather research and operations. The first satellite in the GOES-R series (*GOES-16*) was launched in late 2016, followed by *GOES-17* in early 2018. The GOES-R series also includes replacements for those two satellites, with launches currently listed as late 2021 and early 2025 (https://www.goes-r.gov/mission/mission.html). The ABI (Schmit et al. 2017) has 16 spectral bands with horizontal grid spacing at nadir ranging from 0.5 to 2 km. Its current scan mode ("mode 6") features full-disk scans every 10 min, contiguous United States (CONUS) (from *GOES-16*/GOES-East) or Pacific United States (PACUS) (from *GOES-17*/GOES-West) scans every 5 min, and scans for selected mesoscale domains every 60 s.

The mesoscale domains are movable 1000 km × 1000 km (at nadir) sectors, with the capability of scanning two such sectors per 60 s or one such sector every 30 s. The GLM (Goodman et al. 2013) uses a 777.4-nm wavelength staring charge-coupled device (CCD) imager (1300 by 1372 pixels) with horizontal grid spacing ranging from 8 km at nadir to 14 km near the edges of the field of view. GLM detects lightning flashes based on rapid changes in pixel brightness, using its 2-ms frame rate.

Although GLM's purpose is to detect lightning flashes, it also transmits background visible (777.4 nm) image data for its full field of view, collected at 2.5-min intervals. These background images are distributed as raw digital counts in a standard Level-0 GLM data file, but are not carefully calibrated or geolocated and generally not utilized thus far by research or operations communities. The rapid scans and super rapid scans to which users have grown accustomed from ABI and related imagers on other satellites have proven to be very useful for monitoring rapidly evolving events, such as severe thunderstorms and tropical cyclones (e.g., Velden et al. 1997, 2005; Langland et al. 2009; Bedka et al. 2015; Schmit et al. 2015, 2017; Apke et al. 2016, 2018; Line et al. 2016; Ribeiro et al. 2019; many others). Those scan strategies only cover limited domains (e.g., CONUS, or a temporarily designated mesoscale sector). However, in this paper we explore the rapid (2.5 min) temporal sampling by GLM over broader domains, including most of Central and South America (movie S1 in the online

---

⌀ Denotes content that is immediately available upon publication as open access.

✎ Supplemental information related to this paper is available at the Journals Online website: https://doi.org/10.1175/MWR-D-20-0079.s1.

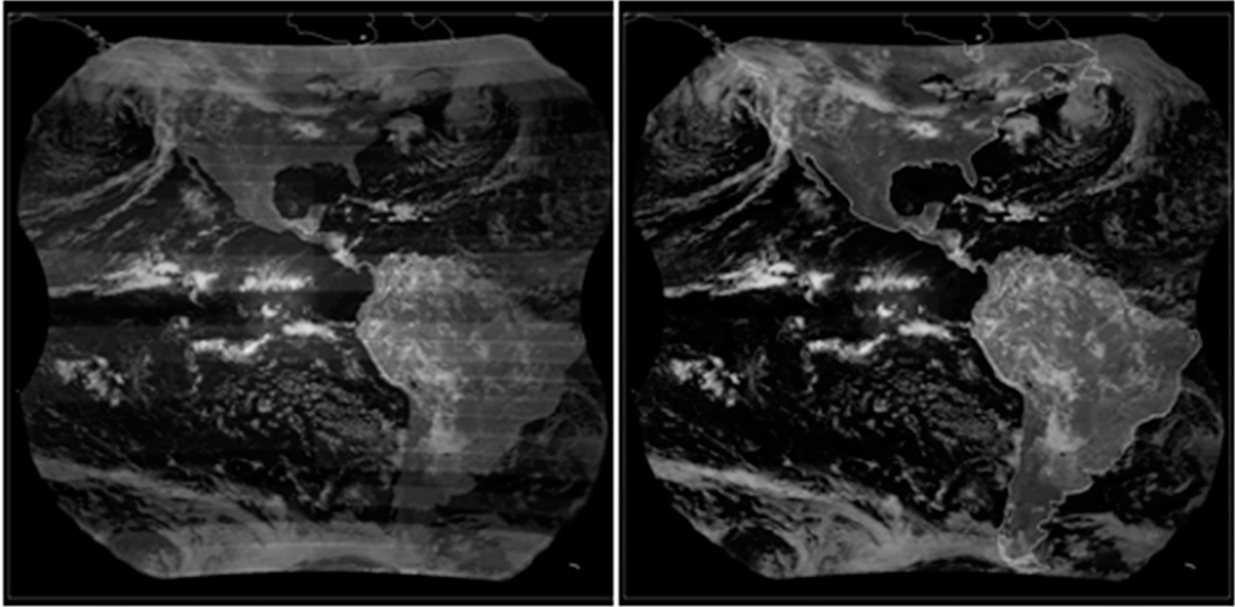*Corresponding author*: Daniel J. Cecil, daniel.j.cecil@nasa.gov

FIG. 1. GLM background scene (a) before and (b) after calibration. This view is from the *GOES-16* checkout phase when it was positioned at 89.5°W. For the operational GOES-East and GOES-West locations, the fields of view are shifted 14.3° east (to 75.2°W) and 47.7° west (to 137.2°W), respectively. For animation of the GOES-East field of view, see movie S1 in the online supplemental material.

supplemental material) where imagery at intervals shorter than 10 min is rarely collected by ABI. Despite coarse horizontal resolution, the animations appear to be useful for monitoring the test cases presented here—a volcanic eruption in Guatemala and a severe thunderstorm complex in Argentina. This paper is intended as an initial proof of concept, demonstrating that the GLM Level-0 background imagery may be an untapped resource worthy of incorporation into research or operational efforts.

2. Data and methods

Raw GLM background images are stored and distributed in standard Level-0 GLM data files (GOES-R Series Program 2019), available from the National Centers for Environmental Information. The GLM 1372 × 1300 pixel CCD array consists of 56 subarrays (each 49 pixels high by 650 pixels wide). Each of the subarrays is read out in parallel to optimize onboard data processing and event detection. Offset biases between subarrays are evident in the raw background image (Fig. 1a), and subarray boundaries are visible as an artifact of data readout. There is no onboard calibration. The calibrated background images shown in Fig. 1b and subsequent figures are obtained from the raw digital numbers by subtracting a dark-offset from a moonless night and applying calibration tables obtained during ground testing (Edgington et al. 2019). The subarray bias adjustments are accounted for in the calibration tables, although some residual instrument biases remain in high contrast situations. The resulting calibrated GLM background images are in units of $mW\,sr^{-1}\,cm^{-2}\,\mu^{-1}$ and appear very similar to visible ABI images at the same time, aside from the differences in horizontal resolution.

Although lightning-flash information is carefully geolocated (van Bezooijen et al. 2016), the GLM files that are distributed do not contain geolocation information for the background images themselves. The initial GLM background geolocation we apply is based on manually matching the locations of distinctive, stationary features (e.g., coastlines). A more robust approach could follow the methodology of van Bezooijen et al. (2016), using spacecraft position, instrument mounting information, and lens assembly temperatures. That has not been attempted in this initial analysis, since the purpose of this paper is to demonstrate that the high temporal resolution available from GLM background imagery does warrant further analysis.

As a first approach, motions in the cloud field were estimated for the Argentina severe thunderstorm case by processing the imagery in the University of Wisconsin Man–Computer Interactive Data Access System (McIDAS), specifically the ''PCMW'' program. PCMW, as run in McIDAS, calculates velocity vectors by making point-to-point measurements as opposed to using correlation tracking of cloud features. For this paper, vector velocities were determined for several selected cloud features that could be manually identified and tracked, as image sets (3–4) were analyzed. This is a subjective approach for acquiring cloud motion vectors, while the motion vectors pertain to the cloud tops. The procedures used in this paper are suitable for a quick, initial 'proof of concept' analysis of cases, demonstrating potential uses of GLM background imagery. Deeper scientific investigation of these or other cases would demand that more rigorous processing methods be applied, as compared with those described here.

Since the GLM backgrounds have coarse (~10 km, varying with distance from nadir) horizontal grid spacing, we compare them with 0.5-km-grid-spacing, 0.64-μm visible imagery from
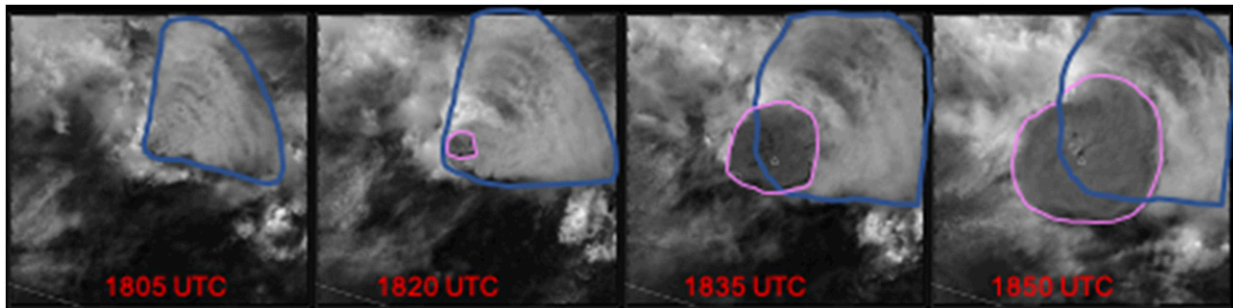
FIG. 2. ABI channel 2 (0.64 μm; visible) imagery between 1805 and 1850 UTC 3 Jun 2018 for the Fuego Volcano case. The ash cloud from early morning is outlined in blue, and the ash cloud from the midday eruption is outlined in pink. Shown is a 1° × 1° box centered on the volcano at 14.47°N, 90.88°W. Scan mode had 15-min intervals for full-disk scans at the time. See also movie S2 in the online supplemental material.

the ABI. ABI data (GOES-R Calibration Working Group and GOES-R Series Program 2017) were obtained online (https://www.bou.class.noaa.gov/saa/products/welcome). For the Fuego Volcano eruption case on 3 June 2018, ABI full-disk scans were available at 15-min intervals. For the Argentina severe thunderstorm case on 10 November 2018, a special ABI mesoscale sector provided imagery every 60 s. This location was otherwise seen at 15-min intervals by the ABI full-disk scans. The ABI scan mode was subsequently changed to allow full-disk scans at 10-min intervals, beginning in April 2019.

3. Fuego Volcano example

The Fuego Volcano at 14.47°N, 90.88°W in Guatemala (also known as Volcan de Fuego; 3763-m summit elevation) had been emitting a low-altitude ash cloud and pyroclastic flows with explosions through the morning of 3 June 2018. The volcano violently erupted around midday (~1800 UTC) and sent an ash cloud to 9-km altitude (Global Volcanism Program 2018a,b). The associated ashfall, lahars, and pyroclastic flows caused at least 190 deaths. The ash cloud itself led to closure of Guatemala's main airport. ABI imagery centered on the volcano is shown in Fig. 2 from before and during the eruption. At 1805 UTC, the region has many meteorological clouds together with a volcanic plume extending toward the north and east. The volcanic plume is manually outlined with a blue line in Fig. 2. At 1820 UTC, a small burst of darker ash (outlined in pink) is centered on the volcano. In the next ABI images at 1835 and 1850 UTC, this burst of darker ash becomes prominent with expansion in all directions.

In the GLM background imagery in movie S2 in the online supplemental material and in Fig. 3, the dark ash cloud is seen as a rapidly expanding set of dark pixels. We have zoomed in to a 1° × 1° box for the sake of keeping the early stages of the eruption easily viewable. This approach gives the unfortunate impression that details of a more typical cloud field cannot be resolved by GLM, but the example in the next section does convey much more detail about convective clouds. The ash plume that was emitted during the morning is indistinct but is outlined in blue in the first panel of Fig. 3 (1816:29 UTC) for reference. Darker ash from the midday eruption is outlined in

pink in Fig. 3, beginning with the 1821:29 UTC panel. Between the times of the 1820 and 1835 UTC ABI images, there are six GLM background images with the pixels near the volcano becoming progressively darker with time. The area of the ash cloud is seen to grow rapidly in the GLM sequence, especially between 1831 and 1851 UTC (middle columns of Fig. 3). As the dark ash cloud expands farther, the pixels nearest the volcano are less dark, both in the ABI and GLM imagery. The eruption imagery is much easier to view in an animation than on the static/printed page. Movie S2 in the online supplemental material shows the 0.5-km, 15-min imagery from ABI side-by-side with the ~10-km, 2.5-min imagery from GLM. While the horizontal detail from ABI gives the more obvious impression of a dark ash cloud, as compared with the appearance of a dark blob from GLM, the 2.5-min updates from GLM fill the temporal gaps for this rapidly evolving scene.

4. Argentina severe thunderstorm example

Northern Argentina and adjoining parts of Brazil, Paraguay, and Uruguay are a hotspot for severe thunderstorms (e.g., Zipser et al. 2006; Cecil and Blankenship 2012; Rasmussen et al. 2014). This helped to motivate the recent Remote sensing of Electrification, Lightning, And Mesoscale/microscale Processes with Adaptive Ground Observations (RELAMPAGO) field program in late 2018. Trapp et al. (2020) describe radar observations of a supercell thunderstorm during RELAMPAGO that produced large (>4 cm), damaging hail on 10 November 2018. Several storms across northern Argentina throughout the day appeared capable of producing severe weather (Fig. 4; movie S3 in the online supplemental material), in addition to the one nearest the field campaign assets that was described by Trapp et al. (2020). On the basis of the hail-retrieval approach of Bang and Cecil (2019) using passive microwave imagers from low-Earth-orbit satellites, three distinct storms were seen at 2151 UTC with hail likelihoods ranging from 54% to 97%, and four more had hail likelihoods exceeding 20%. All seven of those storms easily satisfied the hail detection criteria of Mroz et al. (2017) and Ni et al. (2017) from their 19- and 37-GHz passive microwave brightness temperatures. The RELAMPAGO field catalog also depicts several reports of
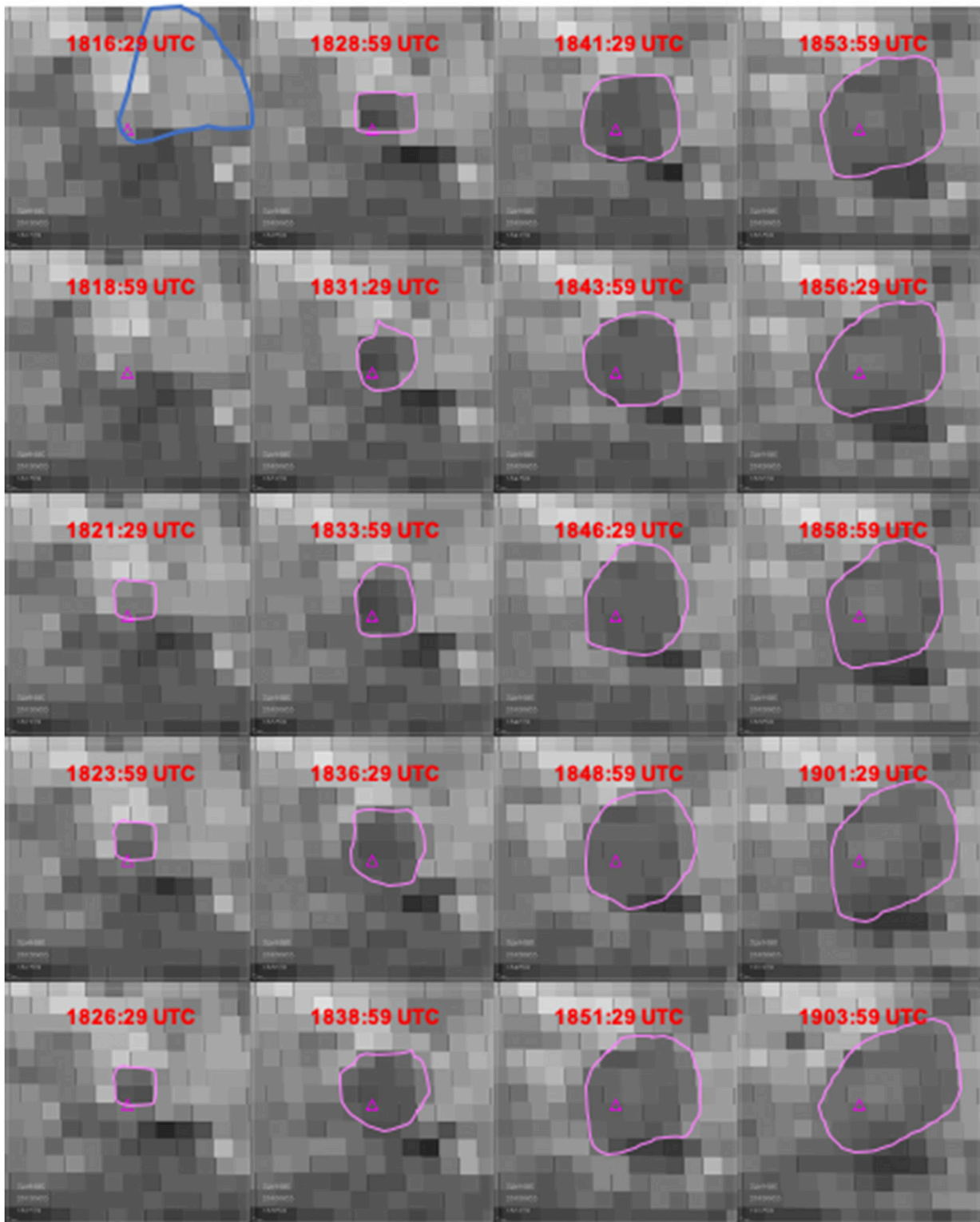
FIG. 3. GLM background images for the Fuego Volcano eruption in Guatemala, 1816:29–1903:59 UTC 3 Jun 2018. Initial geolocation and calibration to the GLM backgrounds have been applied. The ash cloud from early morning is outlined in blue in the first panel only, and the ash cloud from the midday eruption is outlined in pink. The purple triangle marks the location of the volcano's summit. In the first frames on the left, pixels near the volcano have subtle darkening from frame to frame. Darkened pixels from the volcano's ash cloud expand outward with time. See also movie S2 in the online supplemental material.
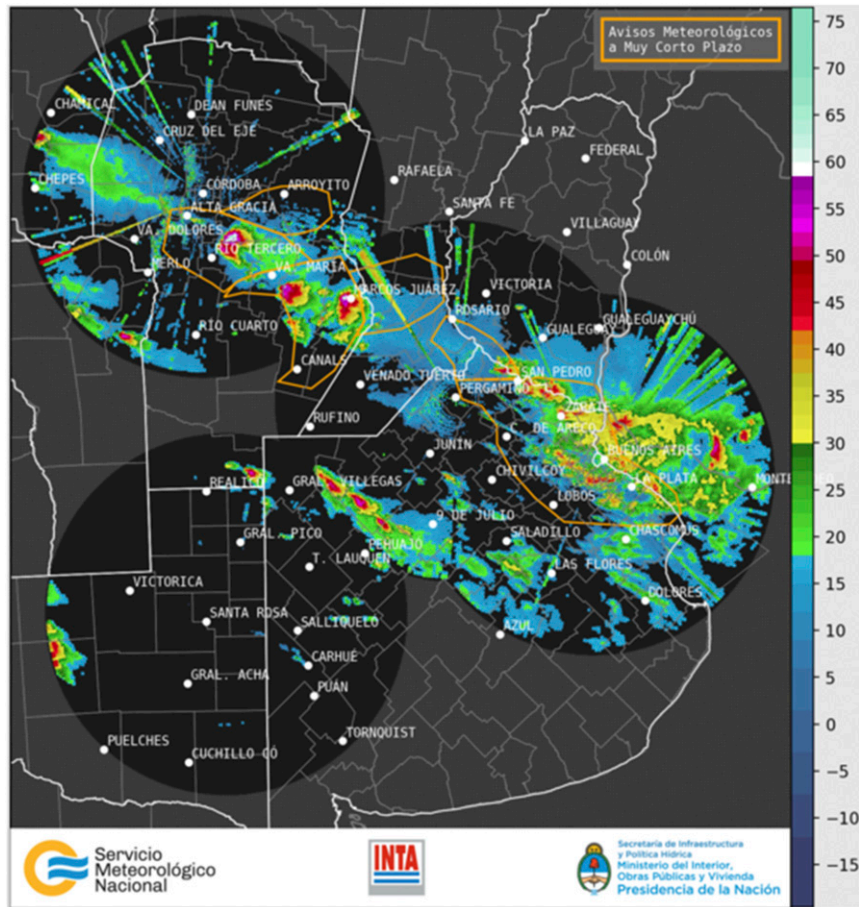
FIG. 4. Quick-look mosaic of radar reflectivity at 2040 UTC 10 Nov 2018 from Argentina's National Meteorological Service. The image is from the catalog of the RELAMPAGO field campaign (http://catalog.eol.ucar.edu/relampago/radar).

hail, strong winds, and heavy rain for this event. These storms formed ahead of an approaching upper-level trough, in an environment with strong vertical wind shear and abundant thermodynamic instability, as shown by Trapp et al. (2020).

A special ABI mesoscale sector was set over northern Argentina during the RELAMPAGO campaign. This allows comparison of the low-spatial-resolution, high-temporal-resolution GLM background imagery for the 10 November 2018 case with high-spatial-resolution imagery from ABI at corresponding times in movie S4 in the online supplemental material. While the fine details of cloud-top texture are striking from ABI, we were surprised and encouraged by the level of detail that can be seen from GLM background imagery. Overshooting tops can be seen in several frames of supplemental movie S4, especially in the central and southeastern-most storm complexes. Those overshooting tops are mostly obscured in Fig. 5 by the lightning locations observed by GLM that are overlayed in red. The animation (supplemental movie S4) shows expansion of the large convective anvils, along with motions of individual cloud-top features. The centermost storm in supplemental movie S4 and Fig. 5 is the hail-producing

supercell documented by Trapp et al. (2020). Dual-Doppler analyses, vertical cross sections, and hail photographs from that storm can be found in Trapp et al. (2020).

Even though 1-min imagery was available from ABI during the RELAMPAGO field campaign for an ∼1000 km × 1000 km mesoscale scan sector, this region is typically only viewed once every 10 min by ABI's full-disk scan. Movie S5 in the online supplemental material pairs ABI images every 10 min with GLM background images every 2.5 min, to simulate what would be more routinely available. A forecaster using imagery such as in supplemental movie S5 would likely rely on ABI's horizontal resolution to pinpoint features such as convective overshoots or low-level boundaries and then look for roughly corresponding features in the GLM background imagery. Then the motion and evolution of those features could be more readily tracked in the GLM background imagery, with its more frequent updates. A forecaster would likely also look at overlays of lightning-flash data from GLM to identify convective cores and their evolution. Lightning is excluded from the online supplemental animations here to avoid clutter, allowing readers to see what level of detail is present in the GLM background imagery itself.
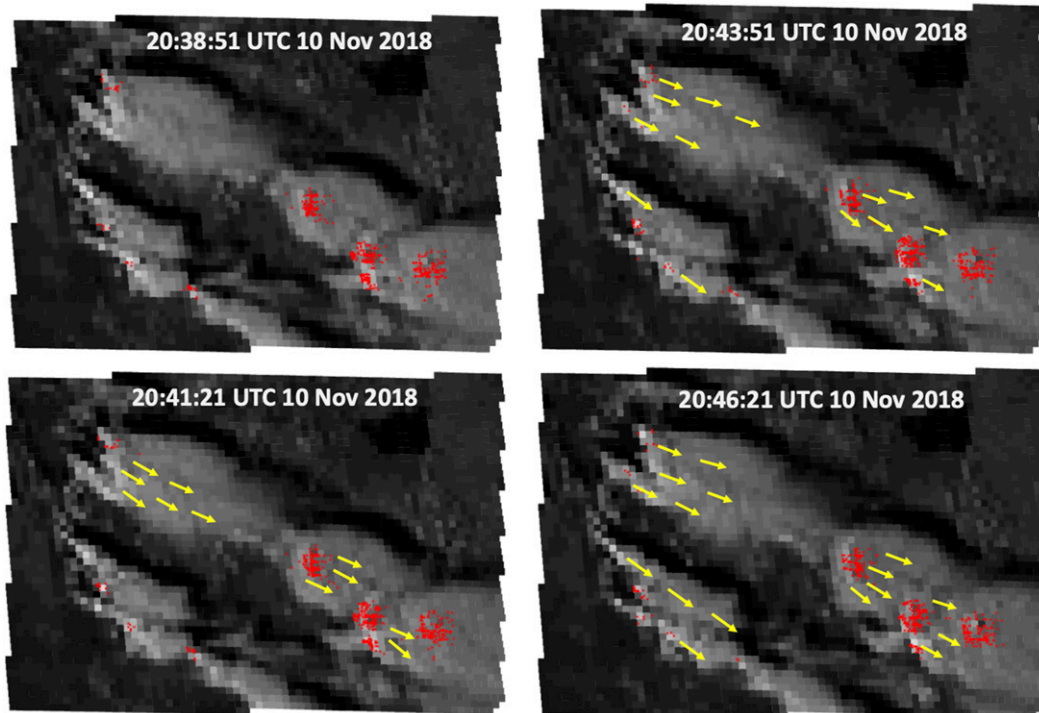
FIG. 5. GLM-derived image offset vectors associated with motions in the cloud field, for the severe thunderstorm case shown in movies S3–S6 in the online supplemental material. GLM lightning-flash locations are plotted in red.

Animation of GLM background imagery over a larger domain and longer time period (movie S6 in the online supplemental material) also shows many features of meteorological interest, despite the coarse horizontal resolution. Terrain features in the west-central and northwestern parts of this domain lead to repeated cloud development in some of the same locations throughout the afternoon. The ongoing morning convection in the south at the beginning of the animation appears to have many associated boundaries, and a westward-propagating outflow boundary emerges after 1700 UTC, south of the main convective complex during the afternoon. Farther north, a cumulus cloud field develops and deepens during the afternoon, with northerly low-level flow subjectively recognizable from the cloud motions. Surface observations (not shown) confirm this inferred moist, northerly flow that is feeding the deep convection farther to the south. Several convective initiation events are captured in the animation, some preceded by orphan anvils from failed attempts at convective initiation. The motion of those small orphan anvils, along with the larger anvils from mature convection, reveals the presence of a strong west-northwesterly upper-level jet. Taken together with the low-level northerly flow across the cumulus field, a forecaster would recognize substantial vertical wind shear from this animation.

To go beyond simple animations of the GLM background imagery, we have made an initial attempt to derive cloud-top motions from a sequence of GLM background imagery (Fig. 5). Image offset vectors depict the prevailing upper-level west-northwesterly flow advecting the convective anvils. They also suggest upper-level diffluence near the overshooting cloud top just to the right of center in these frames. The horizontal grid spacing for the GLM backgrounds makes it difficult to assess the wind speed, and therefore this preliminary analysis really only addresses wind direction. An ~10-km displacement of a cloud feature in 2.5 min would represent a $67\,\text{m s}^{-1}$ speed, which is not a useful level of precision. Higher-quality estimates of wind vectors, with reasonably precise wind speeds, may be possible by eventually merging information from ABI with the GLM background imagery. One could also envision using ABI's multiple infrared bands and derived products to assign heights to vectors that are derived using GLM imagery.

5. Summary

This paper explores a novel use of the GOES-R Series GLM to produce visible imagery over a very large domain (nearly full-disk) with rapid updates (every 2.5 min) (movie S1 in the online supplemental material). For two test cases, a volcanic eruption in Guatemala and a severe thunderstorm complex in Argentina, we have performed an initial calibration and geolocation of the GLM background imagery. Those locations are normally viewed every 10 min by the GOES-R ABI full-disk scan (although the scan mode during these events in 2018 had 15-min intervals between scans). The ABI provides much finer spatial resolution than GLM, but the temporal sampling by GLM appears to add value by filling gaps between ABI scans.

For the Fuego Volcano case shown in movie S2 in the online supplemental material and Figs. 2 and 3, ABI gave 15-min

updates of the appearance of a prominent ash cloud. GLM's ~10-km horizontal grid spacing makes the ash cloud appear to be a dark blob, rapidly expanding outward from the volcano. While the GLM imagery lacks fine horizontal detail, it provides five additional snapshots of the dangerously expanding ash cloud between the times of each pair of ABI images.

For the Argentina severe thunderstorm case in movies S3–S6 in the online supplemental material and Fig. 5, the level of horizontal detail that can be seen in the GLM background imagery is impressive. Overshooting cloud tops and convective structures distinct from the more prominent anvils can be noticed. An initial computation of cloud-top motion in Fig. 5 reveals a combination of upper-level diffluence from the convective regions together with east-southeastward advection of the main cloud features. Qualitative inspection of supplemental movie S6 also suggests northerly flow across a field of low cumulus, likely feeding low-level moisture from the deeper tropics into the region of the storms, with substantial vertical wind shear. Multiple cloud boundaries, likely including convective outflow boundaries, are also seen propagating through the animation. The rapid updates in the GLM background imagery reveal several instances of convective initiation.

These cursory looks at a volcano and a severe thunderstorm case are intended to demonstrate the potential for using rapid-update visible imagery from GLM. The contextual details that can be seen in the thunderstorm case are valuable, despite the imagery being at a relatively coarse horizontal resolution. A forecaster or analyst could recognize ingredients for a severe weather event, such as vertical wind shear, moist low-level inflow, convective initiation, and rapid cloud-top expansion. GLM background imagery is certainly no substitute for the higher spatial (and spectral) resolution available from ABI, but the 2.5-min temporal sampling available from GLM over a broad field of view appears to be very promising for incorporation into research investigations or operational applications. Lightning data, the core purpose of the GLM instrument, would of course add more information for scenes with deep convection. Lightning data are mostly excluded from this paper so as to avoid obscuring the GLM background imagery that is new to most readers. Many investigations or applications could benefit from using GLM lightning, GLM background imagery, and ABI imagery together.

Data availability statement. The data used in this paper are publicly available from the National Centers for Environmental Information, as cited in the references [GOES-R Calibration Working Group and GOES-R Series Program 2017 (https://doi.org/10.7289/V5BV7DSR) and GOES-R Series Program 2019 (https://doi.org/10.25921/qc2r-ps67)]. Radar "quick looks" in Fig.4 and movie S3 in the online supplemental material are from the catalog of the RELAMPAGO field campaign (http://catalog.eol.ucar.edu/relampago/radar).

REFERENCES

Apke, J. M., J. R. Mecikalski, and C. P. Jewett, 2016: Analysis of mesoscale atmospheric flows above mature deep convection using super rapid scan geostationary satellite data. *J. Appl. Meteor. Climatol.*, **55**, 1859–1887, https://doi.org/10.1175/JAMC-D-15-0253.1.

——, ——, K. M. Bedka, E. W. McCaul, C. R. Homeyer, and C. P. Jewett, 2018: Relationships between deep convection updraft characteristics and satellite-based super rapid scan mesoscale atmospheric motion vector-derived flow. *Mon. Wea. Rev.*, **146**, 3461–3480, https://doi.org/10.1175/MWR-D-18-0119.1.

Bang, S. D., and D. J. Cecil, 2019: Constructing a multi-frequency passive microwave hail retrieval and climatology in the GPM domain. *J. Appl. Meteor. Climatol.*, **58**, 1889–1904, https://doi.org/10.1175/JAMC-D-19-0042.1.

Bedka, K. M., C. Wang, R. Rogers, L. D. Carey, W. Feltz, and J. Kanak, 2015: Examining deep convective cloud evolution using total lightning, WSR-88D, and GOES-14 super rapid scan datasets. *Wea. Forecasting*, **30**, 571–590, https://doi.org/10.1175/WAF-D-14-00062.1.

Cecil, D. J., and C. B. Blankenship, 2012: Towards a climatology of severe hail storms as estimated by satellite passive microwave imagers. *J. Climate*, **25**, 687–703, https://doi.org/10.1175/JCLI-D-11-00130.1.

Edgington, S., C. Tillier, and M. Anderson, 2019: Design, calibration, and on-orbit testing of the geostationary lightning mapper on the GOES-R series weather satellite. *Proc. SPIE*, **11180**, 1118040, https://doi.org/10.1117/12.2536063.

Global Volcanism Program, 2018a: Report on Fuego (Guatemala). Weekly Volcanic Activity Rep., 30 May–5 June 2018, S. K. Sennert, Ed., Smithsonian Institution and U.S. Geological Survey, https://volcano.si.edu/showreport.cfm?doi=GVP.WVAR20180530-342090.

——, 2018b: Report on Fuego (Guatemala). Weekly Volcanic Activity Report, 6–12 June 2018, S. K. Sennert, Ed., Smithsonian Institution and U.S. Geological Survey, https://volcano.si.edu/showreport.cfm?doi=GVP.WVAR20180606-342090.

GOES-R Calibration Working Group and GOES-R Series Program, 2017: NOAA GOES-R Series Advanced Baseline Imager (ABI) Level 1b Radiances. NOAA National Centers for Environmental Information, accessed 2 January 2020, https://doi.org/10.7289/V5BV7DSR.

GOES-R Series Program, 2019: NOAA GOES-R Series Geostationary Lightning Mapper (GLM) Level 0 Data. NOAA National Centers for Environmental Information, accessed 31 January 2020, https://doi.org/10.25921/qc2r-ps67.

Goodman, S. J., and Coauthors, 2013: The GOES-R Geostationary Lightning Mapper (GLM). *Atmos. Res.*, **125–126**, 34–49, https://doi.org/10.1016/j.atmosres.2013.01.006.

Langland, R. H., C. Velden, P. M. Pauley, and H. Berger, 2009: Impact of satellite-derived rapid-scan wind observations on numerical model forecasts of Hurricane Katrina. *Mon. Wea. Rev.*, **137**, 1615–1622, https://doi.org/10.1175/2008MWR2627.1.

Line, W., T. J. Schmit, D. T. Lindsey, and S. J. Goodman, 2016: Use of geostationary super rapid scan satellite imagery by the Storm Prediction Center (SPC). *Wea. Forecasting*, **31**, 483–494, https://doi.org/10.1175/WAF-D-15-0135.1.

Mroz, K., A. Battaglia, T. J. Lang, D. J. Cecil, S. Tanelli, and F. Tridon, 2017: Hail detection algorithm for the GPM core satellite sensors. *J. Appl. Meteor. Climatol.*, **56**, 1939–1957, https://doi.org/10.1175/JAMC-D-16-0368.1.

Ni, X., C. Liu, D. J. Cecil, and Q. Zhang, 2017: On the hail detection using satellite passive microwave radiometers and precipitation radar. *J. Appl. Meteor. Climatol.*, **56**, 2693–2709, https://doi.org/10.1175/JAMC-D-17-0065.1.

Rasmussen, K. L., M. D. Zuluaga, and R. A. Houze Jr., 2014: Severe convection and lightning in subtropical South America. *Geophys. Res. Lett.*, **41**, 7359–7366, https://doi.org/10.1002/2014GL061767.

Ribeiro, B. Z., L. A. T. Machado, J. H. Huamán Ch., T. S. Biscaro, E. D. Freitas, K. W. Mozer, and S. J. Goodman, 2019: An evaluation of the *GOES-16* rapid scan for nowcasting in Southeastern Brazil: Analysis of a severe hailstorm case. *Wea. Forecasting*, **34**, 1829–1848, https://doi.org/10.1175/WAF-D-19-0070.1.

Schmit, T. J., and Coauthors, 2015: Rapid Refresh information of significant events: Preparing users for the next generation of geostationary operational satellites. *Bull. Amer. Meteor. Soc.*, **96**, 561–576, https://doi.org/10.1175/BAMS-D-13-00210.1.

——, P. Griffith, M. M. Gunshor, J. M. Daniels, S. J. Goodman, and W. J. Lebair, 2017: A closer look at the ABI on the GOES-R series. *Bull. Amer. Meteor. Soc.*, **98**, 681–698, https://doi.org/10.1175/BAMS-D-15-00230.1.

Trapp, R. J., and Coauthors, 2020: Multiple-platform and multiple-Doppler radar observations of a supercell thunderstorm in South America during RELAMPAGO. *Mon. Wea. Rev.*, **148**, 3225–3241, https://doi.org/10.1175/MWR-D-20-0125.1.

van Bezooijen, R. W. H., H. Demroff, G. Burton, D. Chu, and S. Yang, 2016: Image navigation and registration for the Geostationary Lightning Mapper (GLM). *Proc. SPIE*, **10004**, 100041N, https://doi.org/10.1117/12.2242141.

Velden, C. S., and Coauthors, 2005: Recent innovations in deriving tropospheric winds from meteorological satellites. *Bull. Amer. Meteor. Soc.*, **86**, 205–224, https://doi.org/10.1175/BAMS-86-2-205.

——, C. M. Hayden, S. J. Nieman, W. P. Menzel, S. Wanzong, and J. S. Goerss, 1997: Upper-tropospheric winds derived from geostationary satellite water vapor observations. *Bull. Amer. Meteor. Soc.*, **78**, 173–195, https://doi.org/10.1175/1520-0477(1997)078<0173:UTWDFG>2.0.CO;2.

Zipser, E. J., D. J. Cecil, C. Liu, S. W. Nesbitt, and D. P. Yorty, 2006: Where are the most intense thunderstorms on earth? *Bull. Amer. Meteor. Soc.*, **87**, 1057–1072, https://doi.org/10.1175/BAMS-87-8-1057.